



Assessment of Wellbore Rupture Modes and Influence of Bedding Plane Slip in Deviated Wellbores and Anisotropic Formations

Tsopela, A. and Bere, A.

Rockfield Software Ltd., Ethos, Kings Road, Prince of Wales Dock, Swansea Waterfront, SA1 8AS, UK

Copyright 2020 ARMA, American Rock Mechanics Association

This paper was prepared for presentation at the ARMA/DGS/SEG International Geomechanics Symposium held in Al Khobar, Kingdom of Saudi Arabia, 3–5 November 2020. This paper was selected for presentation at the symposium by an ARMA Technical Program Committee based on a technical and critical review of the paper by a minimum of two technical reviewers. The material, as presented, does not necessarily reflect any position of ARMA/DGS/SEG, its officers, or members. Electronic reproduction, distribution, or storage of any part of this paper for commercial purposes without the written consent of ARMA/DGS/SEG is prohibited. Permission to reproduce in print is restricted to an abstract of not more than 200 words; illustrations may not be copied. The abstract must contain conspicuous acknowledgement of where and by whom the paper was presented.

ABSTRACT: Successful hydrocarbon recovery has become increasingly challenging with the oil and gas industry exploring reservoirs under unfavourable geological conditions. Several operations rely on wellbore stability usually provided by suitable mud-weight. Estimating the operating mud-weight window demands sufficient knowledge of in-situ stress conditions, well trajectory and formation material properties to eliminate instability issues. Instability issues become significantly important when drilling in challenging environments, such as depleted formations, highly deviated wells or strongly heterogeneous formations. Analytical calculations can predict the onset of plastic yielding and damage around a wellbore; however, frequently used criteria have two inherent limitations in not being able to capture 1) complex stress distribution around wellbores deviated from the in-situ stress direction and/or in non-homogeneous formations, and 2) material softening/hardening due to formation damage and redistribution of stress influencing further damage or stability/instability. 3-dimensional numerical modelling combined with advanced constitutive material models can capture stress conditions around wellbores of any orientation as well as non-isotropic characteristics and post-yield strength softening. Using efficient modelling techniques, it is possible to perform detailed wellbore stability analysis for a range of stress conditions, well trajectories and formation anisotropy. Consideration of the results provides beneficial information for drilling, such as operating mud weight window and predicted cuttings volume. In this study, Elfen wellbore software is used to provide detailed assessment of both wellbore deviation and formation anisotropy including bedding plane effects. A representative volume is calculated for each case that corresponds to both the deteriorated material around the wellbore and also undamaged cavings separated from the wellbore surface. The combination of such modelling and results assessment techniques available in Elfen wellbore, aims to enhance current wellbore stability assessments and limit the risks associated with drilling in increasingly difficult conditions.

1. INTRODUCTION

Instability of subsurface excavations is critical and can pose serious problems affecting the timing and success of a project. Prediction of such instabilities has long been recognised as a key factor in many industries. With the oil and gas industry dealing with increasingly challenging geological environments and with complex recovery techniques becoming standard, sufficient prediction and wellbore analysis, requires a wider framework, accounting for difficult geological conditions. Such conditions concern drilling in depleted formations, highly deviated wells or laminated formations. Similar geological environments are also encountered in other applications facing subsurface integrity issues and “reservoir containment geomechanics” (Schultz et al., 2016) such as geothermal fields (Moeck and Bakers, 2011; Ghassemi, 2012) and carbon dioxide sequestration

(Streit and Hillis, 2004; Rutqvist, 2012; Zoback and Gorelick, 2012; Altman et al., 2014).

Wellbore stability prediction, pre-drill and real-time, consists of predicting any instability around the wellbore, based on the stress concentration versus the formation strength. Depending on the mud weight, instabilities affect drilling efficiency, resulting in lost circulation, breakouts or hole closure and even in loss of the open-hole section due to stuck and damaged drill pipe (Lang et al., 2011). Combining methods for real-time wellbore imaging, caving monitoring and managed wellbore pressure with real-time wellbore stability prediction, can significantly improve the planning and management of wells under challenging conditions.

Wellbore stability analysis has been well documented in the published literature (e.g. Zoback 2007) and conventionally it considers the linear elastic or poroelastic response of the rock. Wellbore collapse is expected to

occur at a point surrounding the wellbore whenever the elastic/poroelastic stress satisfies the failure criterion of the rock. Failure criteria such as Mohr-Coulomb or Drucker-Prager can sufficiently predict the onset of plastic yielding. However, these analyses are usually conservative in predicting the mud weight window (Chen and Abousleiman, 2017). Under challenging geological conditions, a more sophisticated representation of the formation response is necessary providing a more appropriate determination of the mud weight window. Therefore, advanced elastoplastic constitutive models accounting for nonlinear hardening or softening behaviour need to be considered in wellbore stability analysis.

Sedimentary rocks are often characterised by laminated structures, most commonly bedding planes. The presence of these structures results in stiffness and strength anisotropy of the bulk formation as shown by numerous experimental studies (e.g. Bonnelye et al., 2017). In-situ observations and experimental results (Willson et al., 1999; Ask and Ask, 2007; Lang et al., 2011; Tellez et al., 2012; Labiouse and Vietor, 2014; Konstantinovskaya et al., 2016; Mehrabian et al., 2018) have shown that in the presence of bedding planes yielding occurs at the corners of the wellbore unlike the conventional breakouts, and the dominant mechanism is buckling of the exposed bedding leading to subsequent fracturing at the maximum curvature (Okland and Cook, 1998). Therefore, conventional considerations of isotropic rock may be insufficient to describe failure when drilling under extended reach wells conditions where bedding-related wellbore instability can become dominant (Ong and Roegiers, 1993).

Semi-analytical solutions are available that consider both strain hardening/softening response (Chen et al., 2012; Gaede et al., 2013; Chen and Abousleiman, 2017) and planes of weakness (Zhang, 2013; Zhou et al., 2018). Nonetheless, these are usually limited to specific types of rock, well orientations or stress conditions. While there exist several numerical models dealing with wellbore stability, only a few of them are able to accurately account for post-yield redistribution of stress around the wellbore and capture progressive damage or instability under complex conditions.

Efficient numerical modelling applied to wellbore stability analysis can capture the mechanism, location and extent of plastic yielding around the wellbore in a range of well trajectories and formation anisotropy. Appropriate consideration of the results provides useful information for drilling including operating mud weight window and predicted cuttings volume. Based on the continuous calculation of the dynamically changing stresses around the wellbore, this information can be provided post-yield.

Such modelling and result assessment techniques are available in the Elfen wellbore software. In the study that

follows, Elfen wellbore software is used to assess wellbore stability in both deviated wells and anisotropic formations providing insight into the different instability mechanisms and estimates cuttings volume prediction making use of the software modelling capabilities. Initially, a horizontal wellbore is considered under different stress and loading conditions reproducing theoretical rupture modes proposed by Etchecopar et al. (1999). Rock anisotropy is then considered by introducing planes of weakness in the model along with a variation of the wellbore trajectory to estimate the effect of wellbore inclination and angle of attack on the deviated wellbore stability. Lastly, a sensitivity study is carried out to assess the impact of varying bedding plane friction angle and stiffness on the dominant failure mechanisms.

2. MODEL SET-UP

Rockfield's 'Elfen wellbore' finite element software is used for the set-up and simulation of the models presented in this paper. A three-dimensional model is used based on the parameters presented in Tsopela et al. (2020). Four theoretical failure modes are initially reproduced as a validation basis for wellbore stability. These failure modes are a function of stress conditions, mud weight and formation strength. The purpose of the wellbore model is to reproduce rupture modes around the wellbore given different stress conditions and mud weight magnitudes, and to explore the effects of anisotropic formation strength and well orientation. The simulations are performed under mechanical, drained analysis.

2.1. Model Geometry

The model consists of a 9.5 inch diameter wellbore, 50 inch long with the boundaries of the domain extending to 95 inch (10×well diameter). In the reference case, the wellbore is considered horizontal with the well axis in the direction of the maximum horizontal stress (Fig. 1).

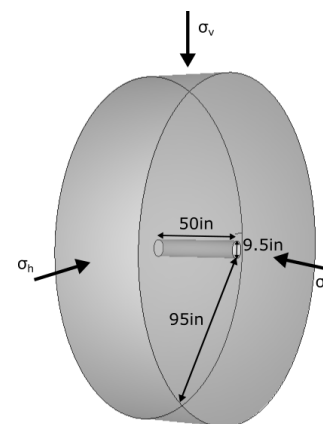


Fig. 1. Model geometry.

The well may be inclined in order to assess the effect of a deviated well and the angle of attack with respect to the in-situ stresses and/or orientation of the planes of

weakness; for this paper the well azimuth of the inclined cases remains in the direction of maximum horizontal stress. Well inclinations and horizontal bedding are shown in Fig. 2, note the in-situ stresses are maintained as parallel and perpendicular to the bedding in all cases. The angles mentioned in Fig. 2 correspond to the well inclinations.

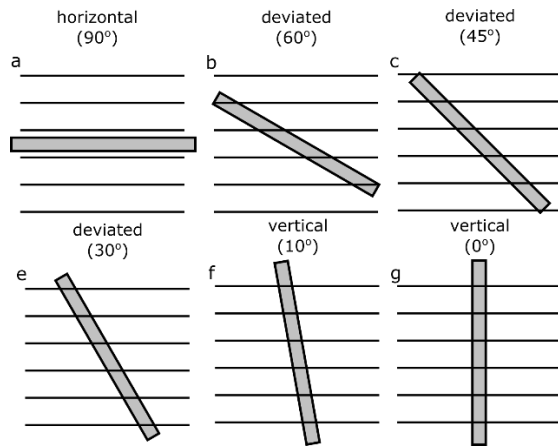


Fig. 2. Well inclination with respect to planes of weakness orientation. Well inclinations are (a) 90°, (b) 60°, (c) 45°, (d) 30°, (e) 10° and (f) 0°.

2.2. Material Properties

Typical sandstone material properties are used in the model to represent the formation, including $\pm 10\%$ stochastically varying elasticity and strength defined by Mohr-Coulomb elasto-plasticity with a Rankine tension cut-off. The post-yield response of the material is captured by accounting for strain-softening through gradual degradation of the cohesion, friction angle and dilation angle as a function of the plastic strain. However, for the D1 case, the shear strength of the material is effectively removed to isolate tensile failure.

To assess the effect of strength anisotropy on wellbore response and failure mode, planes of weakness (PoW) are included in the base case models presented in this study and can be considered a representation of bedding. The PoW properties are represented by 1) elasticity factors normal and tangential to the planes of weakness which are defined as a factor of the host rock Young's and shear moduli, and 2) plastic properties, i.e. cohesion and friction angle. The plastic properties used for the PoW are in the range of values used in the study from Zhang (2013). In addition to strength anisotropy, the effect of PoW friction angle and normal stiffness variation on wellbore instability will be investigated. A summary of the material properties used in the base case model is presented in Table 1. It should be noted that the tensile strength across PoW is considered zero.

Table 1. Host rock and PoW properties

Host Rock Elastic Properties	
Young's Modulus, E (psi)	3e6
Poisson's Ratio, ν (-)	0.2

Density, ρ (g/cc)	0.0058
Host Rock Plastic Properties	
Cohesion, c (psi)	865
Friction Angle, ϕ (°)	30
Dilatancy, ψ , (°)	30
Uniaxial Compressive Strength, UCS (psi)	2995
Tensile Strength, σ_t (psi)	217
Planes of Weakness Elastic Properties	
Stiffness Ratio Normal to PoW, E_w/E (-)	0.5
Stiffness Ratio Tangential to PoW, G_w/G (-)	0.5
Cohesion, c_w (psi)	200
Friction Angle, ϕ_w (°)	15
Tensile Strength, σ_t (psi)	0

2.3. Initial Conditions

According to Etchecopar et al. (1999), under compressional stress states there are six theoretical rupture modes occurring in wellbores sub-aligned to one principal stress direction as shown in Fig. 3. A1 and A2 rupture modes correspond to the common wellbore breakouts with the tangential (or hoop) stress at the wellbore exceeding the strength of the rock. B1 and B2 modes result from excessive axial stress relatively to the internal pressure. Excessive internal pressure relatively to external stress causes the C1 and C2 rupture modes that are believed to form due to elastic deformation in the unruptured parts of the wellbore, without producing cavings. D1 corresponds to the tensile failure of the formation, because of the high mud weight applied. Under such conditions, a tensile fracture is developed, propagating in the direction of the maximum stress and perpendicular to the minimum stress.

Focusing on A1, B1, C1 and D1 rupture modes and based on the resulting drilling stresses responsible for each rupture mode, it is possible to establish the initial in-situ stress state, equivalent circulating density (ECD) and static overbalance for each case. To reproduce the basic rupture patterns, a horizontal well, aligned with a principal stress is considered in this study. Using Anderson's classification (Anderson, 1905), modes A1 and D1 are the result of normal stress regime while B1 and C1 are the result of a strike-slip stress regime. The values of total principal stresses are summarised in Table 2.

Table 2. Principal stress magnitudes, pore pressure, ECD and static overbalance for A1, B1, C1, D1 rupture modes

	A1	B1	C1	D1
Vertical stress, σ_v (psi)	12744.8	10195.7	10195.7	12744.8
Max horizontal stress, σ_H (psi) – aligned N-S with well axis	12744.8	12744.8	12744.8	12744.8

Min horizontal stress, σ_h (psi)	11744.8	9800.7	9800.7	11744.8
In-situ Pore Pressure, P_{form} (psi)	8131.9	8131.9	8131.9	8131.9
ECD (psi)	10000	9000	9000	10000
Static Overbalance (psi)	9000	8650	11500	18000

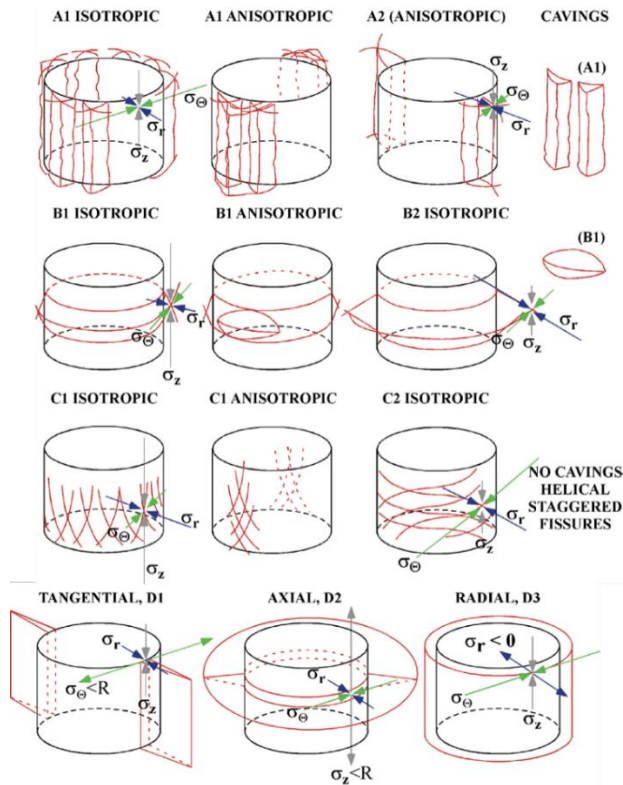


Fig. 3. Shear and tensile rupture modes around a vertical wellbore (after Etchecopar et al. (1999)).

The effect of strength anisotropy (PoW or bedding) is investigated for all stress regimes established. Well inclination and variation of PoW properties is performed under the stress state of case A1 (normal stress regime).

2.4. Loading / Drilling and Analytical Assessment

Loading of the wellbore includes i) the increase of the mud pressure during the excavation of the well, ii) a period of constant pressure higher than the formation pressure, that corresponds to the equivalent circulating density (ECD) and iii) a pressure decrease or increase to a static overbalance. ECD and static overbalance values are different for each case depending on the reproduced failure mode; for all cases the ECD pressure maintains elastic conditions for the excavated wellbore. The loading curves for each case are shown in Fig. 4 (left column); loading curves for cases A1 and B1 show a pressure decrease after ECD while C1 and D1 show a pressure increase. This difference was applied to achieve the

different failure modes, shear for A1, B1 and tensile for C1, D1. It should be noted that in the interest of consistency, wellbore instability only occurs during the change from ECD to static overbalance. Fig. 4 also shows analytical drilling stresses for ECD and static overbalance pressure values along with the Mohr-Coulomb (MC) and/or tensile strength limits as a function of the angle around the well. The angle around the well is defined as $0^\circ/180^\circ$ at the sidewalls and $90^\circ/270^\circ$ at the base and crown of the wellbore. During ECD pressure application, the analytical drilling stress confirm no instabilities occur on the wellbore wall as the shear strength of the material (MC limit) is higher than the stresses for cases A1, B1 and C1. Similarly, with respect to the tensile strength limit, for cases C1 and D1 all wellbore stresses are more compressive.

Due to the anisotropy of the stresses perpendicular to the well axis, the resulting axial and hoop stresses vary as a function of the angle around the well (note the radial stress corresponds to the mud-weight and hence is uniform around the well). Fig. 4 shows that analytically, under A1 conditions, shear failure in the hoop direction will be predominantly at the sidewalls and with a breakout angle of approximately 150° . Under B1 conditions, shear failure will also occur predominantly at the sidewalls but in the axial direction with an equivalent 'breakout' width of approximately 120° . For C1, Fig. 4 indicates that concurrent axial shear and hoop tensile failure will occur at the base and crown of the wellbore. Under D1 conditions, tensile failure in the hoop direction will initiate at the base and crown of the wellbore and cover 140° .

It should be noted that the analytically calculated extent of failure (angles around the wellbore), as presented in Fig. 4, do not consider post-failure material softening or stress redistribution. Due to this limitation the extent of failure is considered excessive and overly-conservative; the simulations results aim to provide a more realistic failure response. This could have a direct impact on mud-weight design whereby breakout widths are considered a constraint (e.g. for vertical wells 90° breakouts are widely considered tolerable).

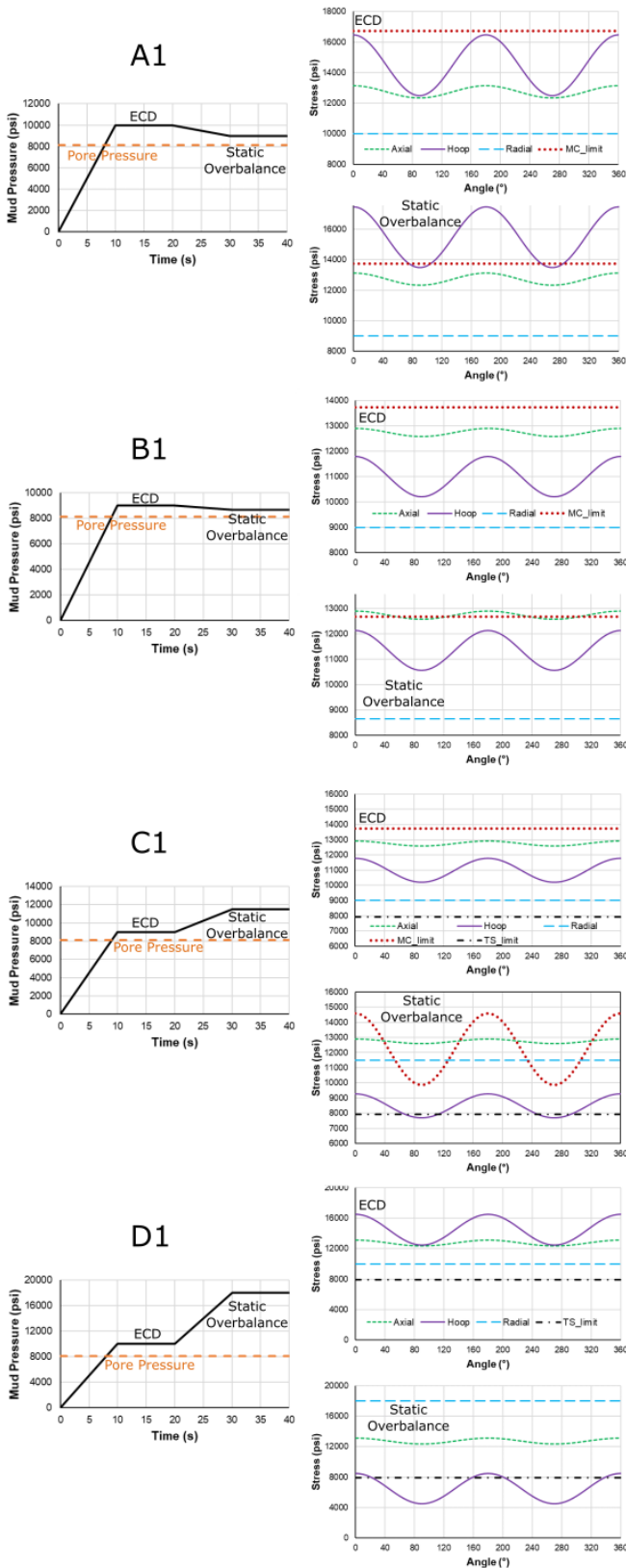


Fig. 4. Loading curve and drilling stresses for ECD and static overbalance for cases A1, B1, C1 and D1; 0° and 180° relate to the well sidewalls.

3. SIMULATION RESULTS

3.1. Horizontal well in isotropic formation

Using the Elfen wellbore software, four different stress and loading configurations were investigated considering a horizontal well aligned with the principal stress directions in an isotropic formation.

In order to demonstrate the post-yield material softening and stress redistribution (mentioned in Section 2.4) which is available in the simulations of this paper but typically not available in analytical solutions, Fig 5 shows the progression of analytical calculations and simulations results from ECD to static overbalance for case A1. It is clear from both analytics and simulations that under ECD conditions the formation remains elastic; also, under initial failure (mud-weight of 9800 psi) a similar breakout width or 30° is predicted. However, as the mud-weight is further reduced (9000 psi) the analytical calculation results in a continually increasing breakout width of up to 150°, whereas the simulation generates shear localisation bands and breakouts are only evident at a width of 74°, approximately ½ that of the analytical solution. The impact of material softening and stress redistribution is demonstrated in the third column, which shows the effective mean stress (rock matrix pressure) for each mud-weight. At the static overbalance it can be seen that the EMS is significantly reduced due to the material shear failure and subsequent softening and stress redistribution. This has the effect of localising shear failure planes which propagate deeper into the formation, which then also redistributes stress further into the formation and restricts further growth of the breakout width.

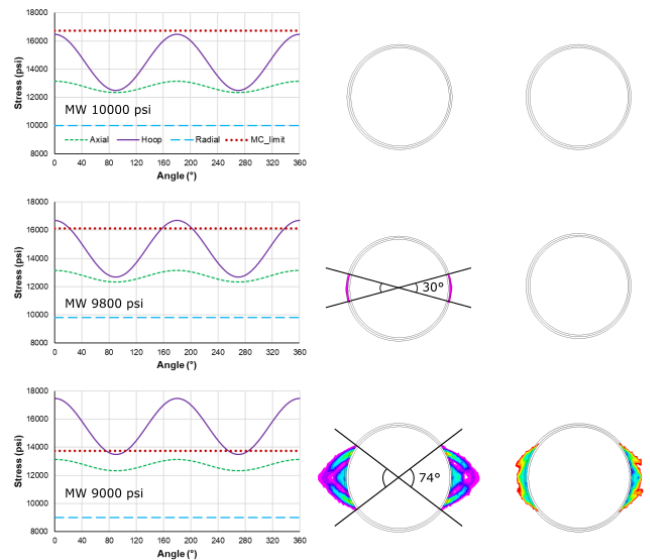


Fig. 5. Left column: Analytical calculations of drilling stresses and Mohr-Coulomb limit; middle column: model effective plastic strain; right column: model effective mean stress at different applied mud weights.

Fig. 6 presents the results for all cases A1, B1, C1 and D1. The first column in Fig. 6 (Fig. 6a, e, i, m) shows a vertical section of the effective plastic strain around the wellbore at the end of ECD; the second column (Fig. 6b, f, j, n)

shows the same at the end of the static overbalance. The third contour plot (Fig. 6d, h, l, p) illustrates a horizontal section of the well at the end of static overbalance. The final set of results (Fig. 6 c, g, k, o) shows the wellbore surface for 0-to-360° angle around the wellbore, whereby 0/180° are the wellbore sidewalls. The analyses described in this section serves as a validation exercise before considering more complex scenarios, challenging to predict analytically.

Based on the rupture modes illustrated in Fig. 3, it is shown that all four failure patterns are well reproduced in our model. A1 configuration considers a normal stress regime and results to the well-known breakout type of failure (Fig. 6b). The drilling stresses correspond to a maximum tangential stress, an intermediate vertical stress and a minimum radial stress. The cavings appear on the wellbore sidewalls, where the tangential stress is expected to be a maximum. The cavings are developing parallel to the well axis (horizontally) as shown in Fig. 6c. it should be noted that both at the end of excavation and ECD, the effective plastic strain is zero, meaning that the well is stable before static overbalance.

The stress regime in B1 configuration is characterised as strike-slip, with the maximum horizontal stress (well axial direction) being the highest. Regarding the resulting drilling stresses, the axial stress is now the maximum stress, the hoop stress intermediate and the radial stress minimum (see also Fig. 4). At the end of the static overbalance, the section of the plastic strain shown in Fig. 6f appears different to the pattern observed in configuration A1 and can be better visualised in Fig. 6 g. The cavings in this case is a result of the high axial stress and is represented in hoop patterns which are more concentrated on the sidewalls.

For C1 configuration, the resulting axial stress is the highest, the radial is the intermediate, due to the elevated mud weight and the hoop is the minimum. Under these conditions, the rupture mode consists of helical tensile/shear fractures as illustrated in Fig. 6l and k. The fractures will develop on the wellbore base and crown where the hoop stress is expected to be a minimum. These fractures appear only on the surface of the well and are unlikely to produce significant deteriorated material volumes like rupture modes A1 and B1. However, well fluid loss could be expected and induced fractures could propagate. It can be seen in Fig. 6i, j, k that small fractures are developing as a result of the increased mud weight applied. Nevertheless, because of the large difference between the vertical and the minimum horizontal stress, these fractures initiate more dominantly as shear fractures on the surface of the well as shown in Fig. 6l. It should be noted that this is illustrated to promote an alternative failure mode suitable for injector fracture/damage initiation.

D1 case corresponds to the well-known tensile fractures where the stress exceeds the tensile strength of the material and would tend to propagate in the direction of maximum stress (perpendicular to the minimum in-situ stress). Similarly, the fractures develop on the wellbore base and crown.

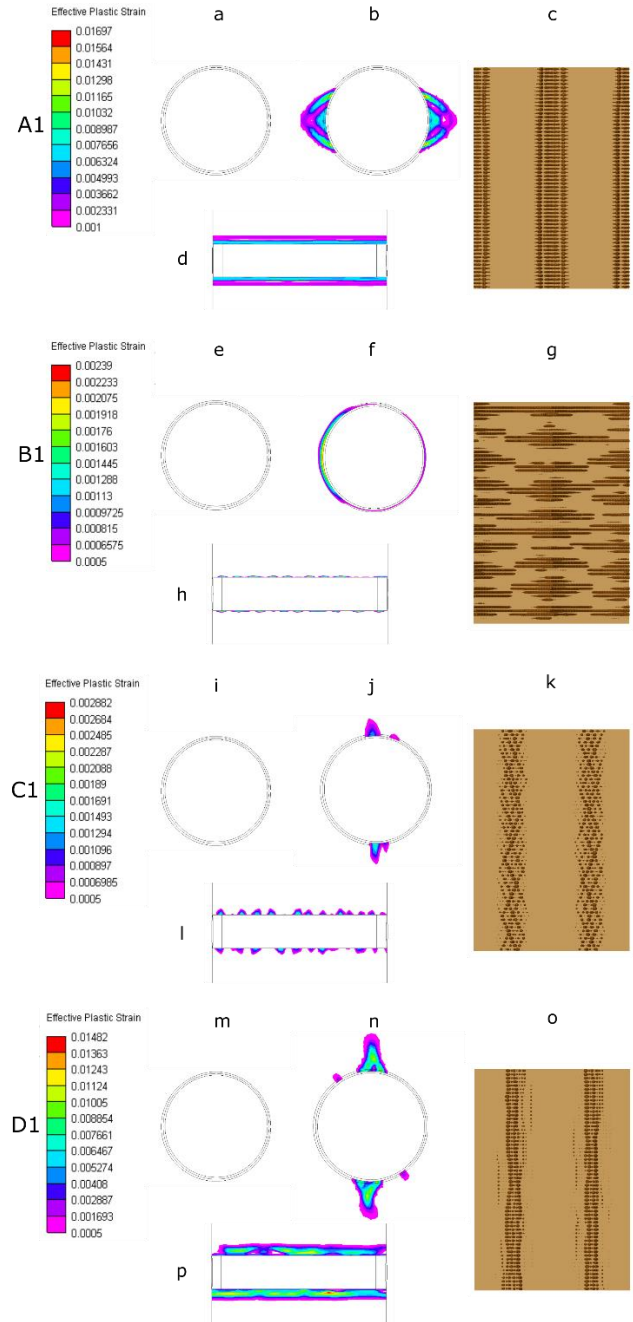


Fig. 6. Effective plastic for A1: (a) section perpendicular to the well axis at the end of ECD, (b) section perpendicular to the well axis, (c) horizontal section, (d) wellbore surface at the end of static overbalance; B1: (e) section perpendicular to the well axis at the end of ECD, (f) section perpendicular to the well axis, (g) horizontal section, (h) wellbore surface at the end of static overbalance; C1: (i) section perpendicular to the well axis at the end of ECD, (j) section perpendicular to the well axis, (k) horizontal section, (l) wellbore surface at the end of static overbalance.

3.2. Horizontal well in anisotropic formation

Planes of weakness are introduced in the model to account for strength anisotropy of the formation, such as bedding planes. The effect of strength anisotropy is investigated for all four configurations A1, B1, C1 and D1 considering the no changes to initial conditions or loading. Horizontal bedding is considered most onerous for a horizontal well (see Fig. 2a); this is considered as producing an angle of attack of 0° . Inclination of the well in an anisotropic formation is described in Section 3.4.

The calculated effective plastic strain and PoW sliding plastic strain for a horizontal well are illustrated in Fig. 7. The effective plastic strain isolates the damage induced to the formation matrix, whereas the sliding plastic strain refers to the post-yield strain accrued in the direction of the bedding (PoW).

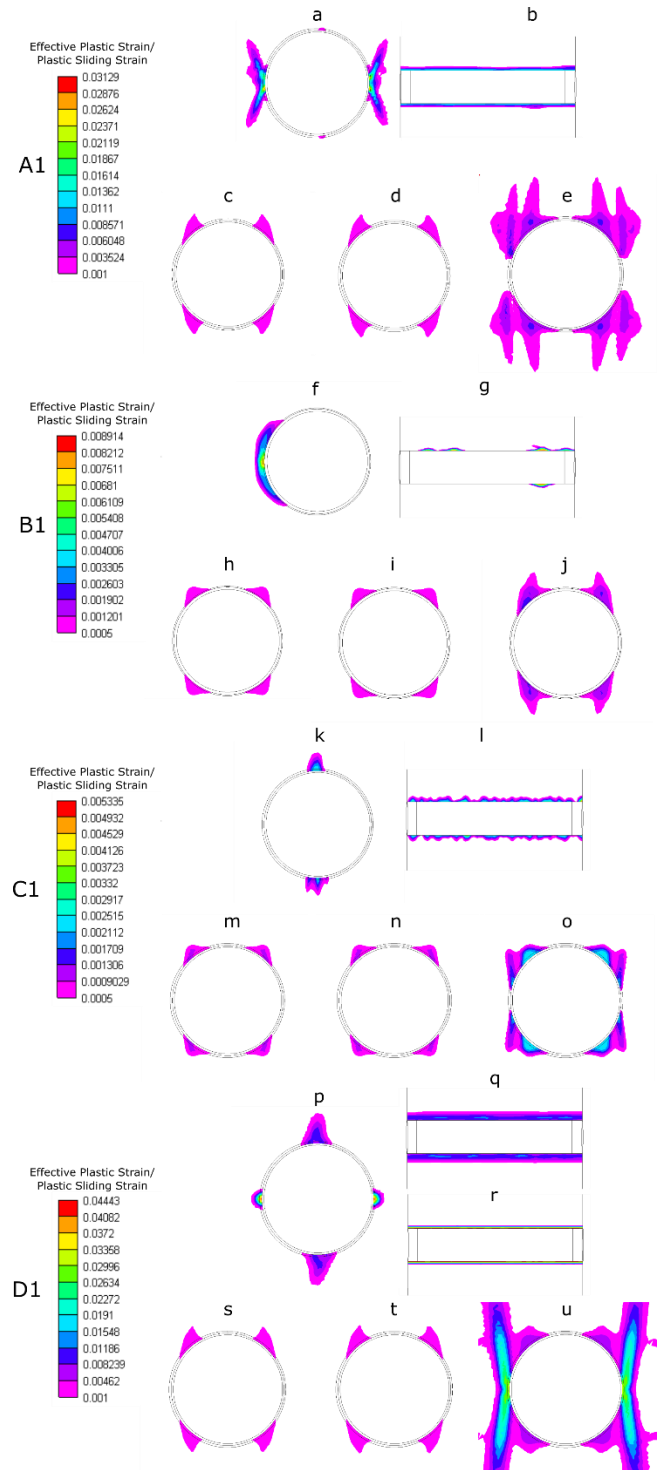


Fig. 7. Effective plastic strain for A1: (a) vertical section, (b) horizontal section at the end of static overbalance, sliding plastic strain for A1 vertical section at the end of (c) excavation, (d) ECD, (e) static overbalance; Effective plastic strain for B1: (f) vertical section, (g) horizontal section at the end of static overbalance, sliding plastic strain for B1 vertical section at the end of (h) excavation, (i) ECD, (j) static overbalance; Effective plastic strain for C1: (k) vertical section, (l) horizontal section at the end of static overbalance, sliding plastic strain for C1 vertical section at the end of (m) excavation, (n) ECD, (o) static overbalance; Effective plastic strain for D1: (p) vertical section, (q) horizontal section (max stress direction), (r) horizontal section (min stress direction) at the end of static overbalance,

sliding plastic strain for D1 vertical section at the end of (s) excavation, (t) ECD, (u) static overbalance.

Strength anisotropy does not significantly affect the basic failure patterns observed for the cases described. However, for all four cases, the maximum effective plastic strain is higher for the configurations accounting for PoW. Focusing on the effective plastic strain, ‘reverse’ cavings develop in case A1 due to the presence of PoW in which damage is initiated at the sidewalls, but then propagated vertically into the formation rather than laterally as for the homogeneous case. The shape of the damage and hence cavings is affected by the sliding and resulting buckling mechanism of the bedding planes (Fig. 8 left) resulting in hinges formed where the effective plastic strain develops. A similar failure pattern is observed in case B1, with and without the PoW. As the axial stress is the highest in this case and strain does not develop far into the formation, it is considered that minimal shearing of the PoW results in fewer cavings.

C1 failure pattern is not affected by the presence of the bedding planes; this is considered reasonable since the formation damage is local to the wellbore surface and acts in an axial direction. For D1, tensile fractures are developing similar to the isotropic formation case. However, an area of high effective plastic strain is developed at the sidewalls (Fig. 7p, r), related to PoW deformation as described below.

While for all cases the host rock fails when the static overbalance pressure is applied, sliding along the bedding planes occurs at an early time, as shown in Fig. 7c, h, m, s illustrating plastic strain at the end of excavation. It should be noted that the PoW shear strength is less than that of the matrix (Table 1). Similar sliding is observed at the end of ECD (Fig. 7d, i, n, t). PoW sliding occurs at locations around the well where the stress conditions encourage the most bedding buckling and plane slip. For such angles of attack, in this case 0°, the dominant failure mechanism is slip along the planes with the well-known buckling and fracturing in the direction normal to the planes of weakness. Regarding D1 configuration, high plastic strain is observed at the sidewalls of the well (Fig. 7p, r, u). This is attributed to the high mud weight applied that can eventually result in the opening of the bedding planes as shown schematically in Fig. 8 (right). Contrary to bedding slip under compressive environments (Fig. 8 left), under tension (or expansion), the bedding planes bend upwards/downwards creating an area of maximum tension at the sidewalls. Such deformation pattern is of particular interest as the opening of bedding planes close to the well surface can potentially create flow paths leading to fluid loss through planes of weakness.

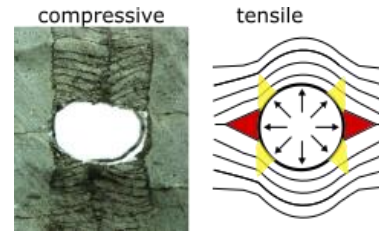


Fig. 8. Left: bedding-controlled fracture pattern under compressive failure (Labiouse and Vietor, 2014); right: opening and bending of bedding under tensile failure.

During all simulations, the continuously changing stresses around the wellbore were calculated and it was possible to capture the post-yield behaviour of the material. It was therefore possible to track and calculate the volume of the elements around the wellbore initially yielding and subsequently experiencing strain softening. As the wellbore surface becomes damaged a criterion is used to determine the elements that no longer support high stresses and their volumes are calculated. This corresponds to both the deteriorated material around the wellbore and also undamaged cavings that are ‘separated’ from the wellbore surface; hence this calculation can provide an estimation of the additional expected cavings volume under specific conditions (in excess of the drilled wellbore). The criterion used for the calculation of the elements volume considers the elements characterised by an effective mean stress $EMS < 2000$ psi. Fig. 9 summarises and compares the volumes calculated for the base cases A1 and B1 with and without PoW. C1 and D1 cases were not considered in the volume calculations since surface and tensile fractures are developing, not accompanied by significant volumetric changes.

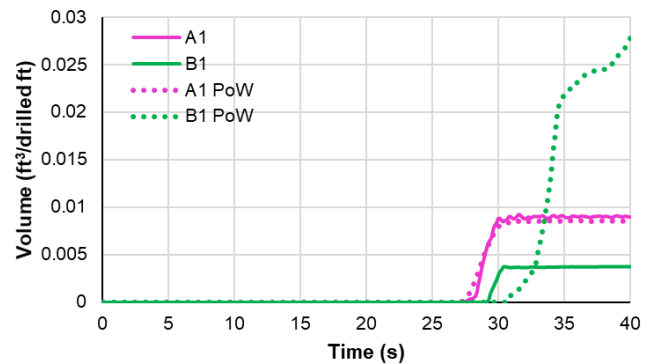


Fig. 9. Calculated total volume of elements per drilled foot with an effective mean stress < 2000 psi for A1 and B1 with and without PoW.

As expected, Fig. 9 shows that for isotropic formation, the largest volume of deteriorated material is produced for case A1. Generally, the development of cavings parallel to the well axis (vertically) leads to larger volumes of deteriorated material. For anisotropic formation, A1 calculated volume is similar to the isotropic case while B1 volume appears to be higher than the isotropic case. The

failure in case B1 consists of a series of damaged hoops which result in reduced axial stress – if the stress reduction is sufficient this will have a continual knock on effect for the adjacent material in the axial direction. This appears to be the cases in anisotropic formations where damage is further concentrated on the sidewalls and hence rapidly the entire model length is exposed to a stress reduction. In the field, material variations along the well are expected to interrupt this knock-on effect.

3.3. Deviated well in anisotropic formation

In this section, and only under the stress and loading conditions corresponding to A1 case, the well is inclined to represent 0° (vertical well), 10°, 30°, 45°, 60° and 90° (horizontal well, base case) in an anisotropic formation (see Fig. 2). Considering horizontal bedding planes, these well inclinations correspond to attack angles of 90°, 80°, 60°, 45°, 30° and 0° (see Fig. 2). It should be noted that since the vertical stress and maximum horizontal (well azimuth) are equal, the influence of well inclination is attributed to attack angle of bedding only as the stress conditions effectively remain unchanged.

Fig. 10 summarises the calculated effective plastic strain (Fig. 10a, c, e, g, i, k) and sliding plastic strain (Fig. 10b, d, f, h, j, l). For high angles of attack ($\theta > 80^\circ$) and therefore low well inclinations, there is no significant slip along the bedding planes as this is considered the safest combination of well and beddings orientation (Okland and Cook, 1998). As the well inclination increases and the angle of attack decreases, it can be seen that the area affected by bedding slip becomes larger. In terms of effective plastic strain, for a well inclination of 90°, ‘reverse’ cavings develop as described in section 3.2. For the rest of the inclinations considered, the failure pattern corresponds to the well-known breakouts on the sidewalls, with the volume of damage decreasing as the well inclination decreases. For well inclinations 0° and 10°, a small amount of plastic strain is also observed at the wellbore base and crown. This is attributed to stress redistribution due to the reduced elasticity of the bedding planes which transfers a greater shear stress demand on the formation matrix.

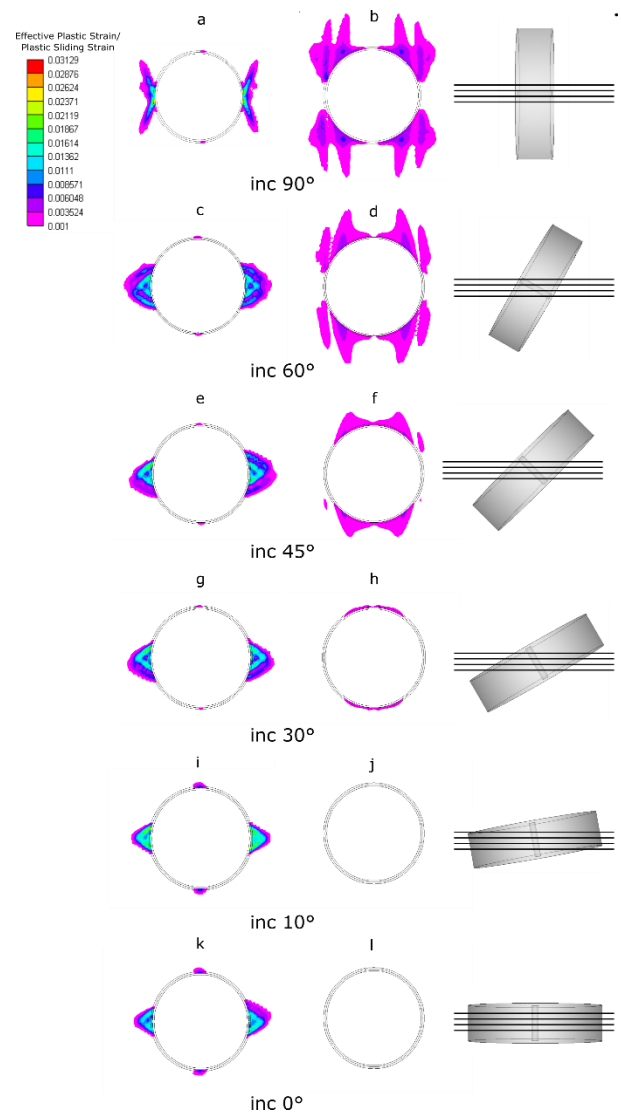


Fig. 10. Well inclination 90°: (a) effective plastic strain, (b) sliding plastic strain; well inclination 60°: (c) effective plastic strain, (d) sliding plastic strain; well inclination 45°: (e) effective plastic strain, (f) sliding plastic strain; well inclination 30°: (g) effective plastic strain, (h) sliding plastic strain; well inclination 10°: (i) effective plastic strain, (j) sliding plastic strain; well inclination 0°: (k) effective plastic strain, (l) sliding plastic strain.

Fig. 11 summarises the calculated cavings volume for all well inclinations considered in an anisotropic formation.

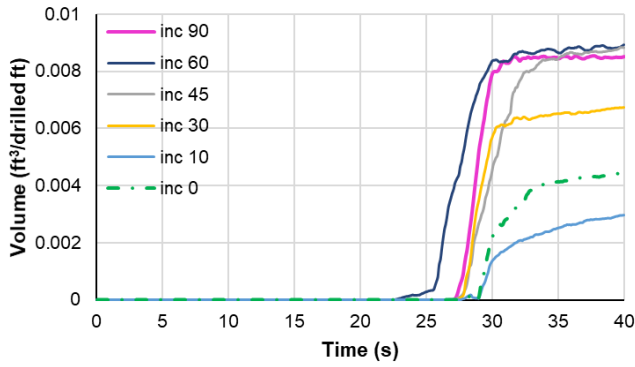


Fig. 11. Calculated total volume of elements per drilled foot with an effective mean stress < 2000 psi for well inclinations 90°, 60°, 45°, 30°, 10°.

Fig. 11 shows that the largest calculated volume corresponds to 60° well inclination characterised by significant cavings volume and bedding slip which induces stress redistribution. Well inclinations of 90° and 45° show similar cavings volumes with different failure mechanisms as described above, i.e. ‘reverse’ cavings and high bedding slip for 90° and normal cavings and limited bedding slip for 45°. Inclinations 30°, 10° and 0° (vertical well) result in very similar cavings volumes with little or no bedding slip and cavings developing in the preferred direction.

3.4. Horizontal well in anisotropic formation – Effect of planes of weakness properties

The effect of PoW properties is investigated in this section through the variation of the friction angle and the normal and shear stiffness of the bedding planes. Similar to section 3.3, the following sensitivity study is performed under the stress and loading conditions of the A1 case.

3.4.1. PoW friction angle

Given a value of 15° as a base case, the friction angle is varied for a range of 10-30°. For a friction angle of 30°, the PoW and the host rock are characterised by the same friction angle (although different cohesions, formation 865 psi, and PoW 200 psi). The effective plastic strain and plastic sliding strain calculated for each friction angle are shown in Fig. 12.

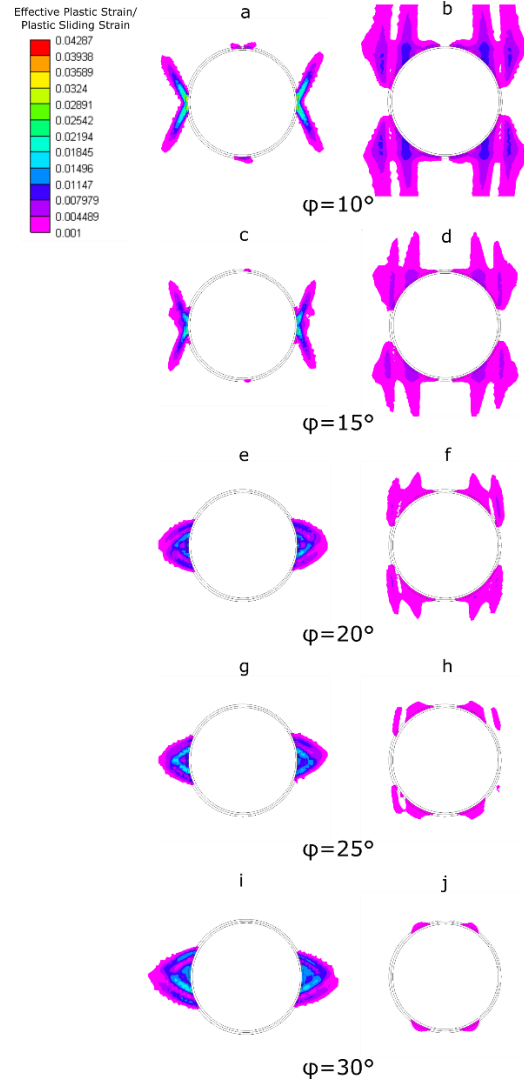


Fig. 12. PoW friction 10°: (a) effective plastic strain, (b) sliding plastic strain; PoW friction 15°: (c) effective plastic strain, (d) sliding plastic strain; PoW friction 20°: (e) effective plastic strain, (f) sliding plastic strain; PoW friction 25°: (g) effective plastic strain, (h) sliding plastic strain; PoW friction 30°: (i) effective plastic strain, (j) sliding plastic strain.

For low friction angles ($\varphi < 20^\circ$), failure of the host rock is characterised by ‘reverse’ cavings as described above (Fig. 12a, c). As expected, the plastic sliding strain is higher and affects a larger volume around the well for a very low friction angle ($\varphi = 10^\circ$) and appears to result in a double buckling failure mode. For higher PoW friction angles ($\varphi \geq 20^\circ$), the bedding slip is significantly reduced and the cavings transition to the well-known breakout type failure (Fig. 12e, g, i). For higher friction angles, slip becomes limited (Fig. 12h, j) and almost insignificant for a PoW friction angle equal to that of the host rock (Fig. 12j); slip still exists for $\varphi = 30^\circ$ since the bedding cohesion is less than that for the formation.

Regarding the cavings volume around the well, Fig. 13 shows that the highest calculated volume corresponds to the lowest friction angle ($\varphi = 10^\circ$) due to high bedding slip, buckling of the bedding, plastic hinge formation and

associated stress relaxation. The second largest volume is observed for the highest friction angle ($\phi=30^\circ$) where the produced volume corresponds to the progressively damaged material of the formed cavings with very little bedding slip that does not contribute to any volumetric changes. The calculated volumes for the rest of the friction angles increase as the friction angle increases. It is obvious that the produced cavings volume is the result of the competition of different dominant failure mechanisms with the two extreme friction values showing the largest volumes.

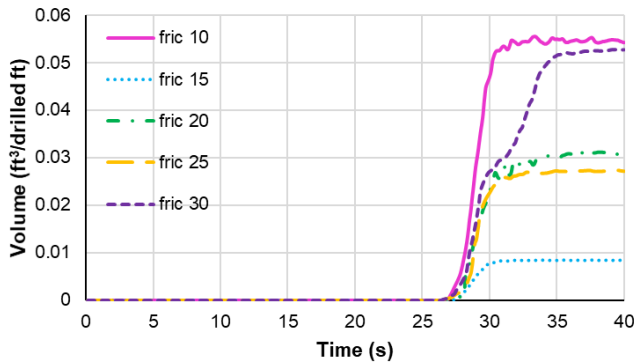


Fig. 13. Calculated total volume of elements per drilled foot with an effective mean stress <2000 psi for PoW friction angles 10°, 15°, 20°, 25°, 30°.

3.4.2. PoW stiffness

Investigating the effect of PoW elastic response, normal stiffness is varied for a range of 0.1-to-0.9 with the reference value being 0.5. It is reminded that the stiffness value is defined as a factor of the host rock Young's and shear moduli. The ratios and corresponding PoW normal and tangential stiffness values are listed in Table 3 below:

Table 3. Stiffness ratios and corresponding values of PoW normal and tangential stiffness.

Ew/E (-)	Normal stiffness (psi)	Tangential stiffness (psi)
0.1	3e5	1.25e5
0.3	9e5	3.75e5
0.5	1.5e6	6.25e5
0.7	2.1e6	8.75e5
0.9	2.7e6	1.125e6

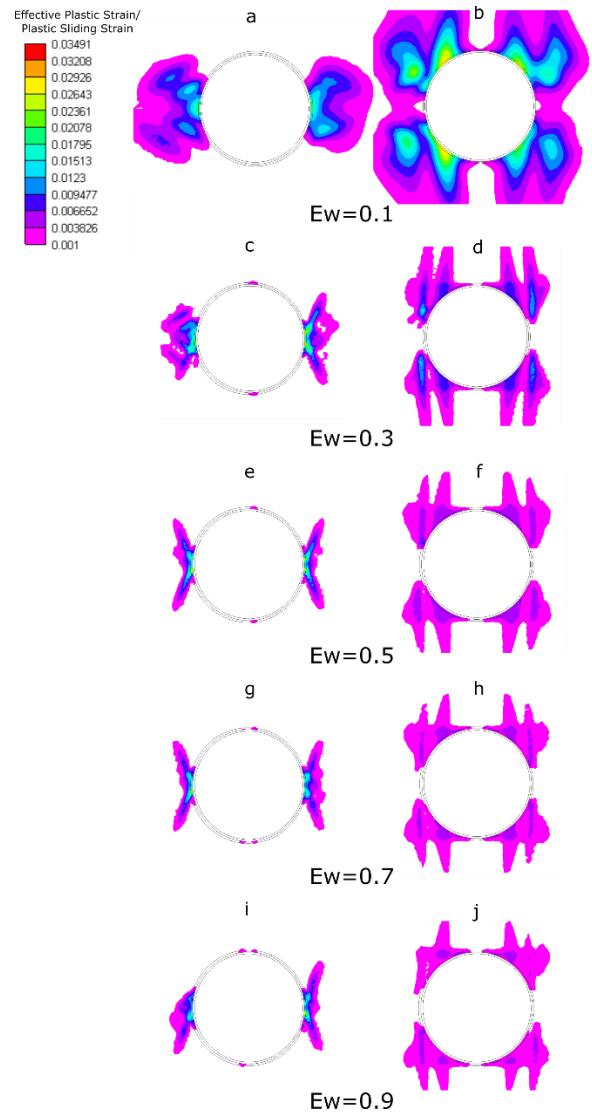


Fig. 14. PoW stiffness ratio 0.1: (a) effective plastic strain, (b) sliding plastic strain; PoW stiffness ratio 0.3: (c) effective plastic strain, (d) sliding plastic strain; PoW stiffness ratio 0.5: (e) effective plastic strain, (f) sliding plastic strain; PoW stiffness ratio 0.7: (g) effective plastic strain, (h) sliding plastic strain; PoW stiffness ratio 0.9: (i) effective plastic strain, (j) sliding plastic strain.

A similar failure pattern is observed for most stiffness ratios considered, as this is mainly dictated by the plastic response of the bedding planes, i.e. irreversible sliding. For low stiffness ratios, ($E_w < 0.5$), i.e. soft bedding planes, a larger cavings volume develops around the wellbore due to high normal and shear strain (Fig. 14a, c). Considering higher stiffness ratios ($E_w \geq 0.5$), the failure pattern is similar to that of the base case (Fig. 14e, g, i) showing 'reverse' cavings as the elastic normal and shear strain become limited. Similarly, sliding plastic strain associated with PoW slip shows the same pattern for all stiffness ratios examined with the highest strain and larger cavings volume recorded for the softer bedding planes.

Similar to the observations made based on plastic strain, Fig. 15 shows that the cavings volume recorded increases as the PoW stiffness decreases. The volume for $E_w=0.1$ is much larger than the rest of the cases (this is considered an extreme contrast in stiffness) while for $E_w \geq 0.5$, the calculated volumes are very similar with the elastic response of the bedding having very little impact.

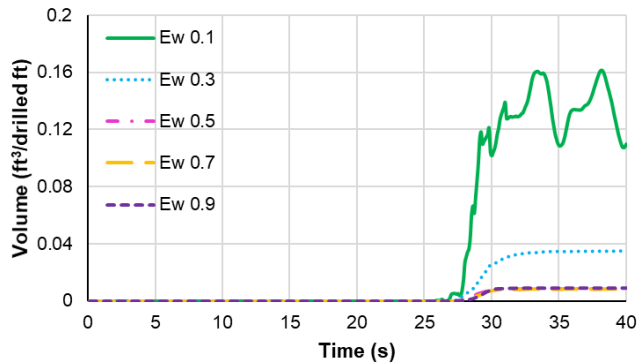


Fig. 15. Calculated total volume of elements per drilled foot with an effective mean stress < 2000 psi for PoW stiffness ratios 0.1, 0.3, 0.5, 0.7, 0.9.

4. CONCLUSIONS

Wellbore instability can pose serious problems in the drilling industry affecting many applications such as hydrocarbon recovery, CO₂ storage and enhanced geothermal systems amongst others. Numerical modelling consists of a robust tool for predicting instability issues that can arise under unfavourable in-situ conditions which are hard to assess analytically. In this study we use the Elfen wellbore software to investigate complex failure modes occurring when drilling in challenging environments. After validating the software against theoretical rupture modes, a sensitivity study was presented where the well alignment was varied with respect to the principal stress directions, drilled in a heterogeneous formation characterised by the presence of planes of weakness and a combination of both the above. The failure patterns observed for the configurations investigated were presented for a given interval of the wellbore considering uniform materials and stress conditions. It was observed that there is competition between formation failure and bedding plane slip induced failure, such as buckling. This competition can change the pattern of failure model and the magnitude of cavings.

Efficient modelling, as presented, allows for multiple sensitivity simulations to be conducted to investigate the influence of sub-surface uncertainties. Additionally, simulations can be used to back-analyse image logs of wellbore surface shear and tensile fractures to provide insight into aspects such as stress state.

As an extension to this study, it would be interesting to vary the rock properties along the wellbore length and assess the possible difference in the failure modes.

Making use of the software capabilities, it is possible to capture not only the failure patterns but also the post-yield softening response of the material and thus the dynamically changing stresses around the wellbore. With this information, we are able to calculate a representative volume corresponding to both the deteriorated material around the wellbore and also undamaged cavings that are separated from the wellbore surface. This can provide useful estimations of the cuttings volume during drilling informing on the extent of instability. The combination of such modelling, results assessment techniques and real-time field monitoring can significantly limit the risks associated with drilling in increasingly difficult conditions.

REFERENCES

- Altman, S.J., B. Aminzadeh, M.T. Balhoff, P.C. Bennett, S.L. Bryant, M.B. Cardenas, K. Chaudhary, R.T. Cygan, W. Deng, T. Dewers, D.A. DiCarlo, P. Eichhubl, M.A. Hesse, C. Huh, E.N. Matteo, Y. Mehmani, C.M. Tenney, and H. Yoon, 2014. Chemical and hydrodynamic mechanisms for long-term geological carbon storage. *J. Phys. Chem.* 118: 15,103–15,113.
- Anderson, E. M. (1905). The dynamics of faulting. *Transactions of the Edinburgh Geological Society*, 8(3), 387-402.
- Ask, D., & Ask, M. V. S. (2006). Detection of potential borehole breakouts in boreholes KFM01A and KFM01B. *SKB P-report in prep.*
- Bonnelye, A., Schubnel, A., David, C., Henry, P., Guglielmi, Y., Gout, C., ... & Dick, P. (2017). Strength anisotropy of shales deformed under uppermost crustal conditions. *Journal of Geophysical Research: Solid Earth*, 122(1), 110-129.
- Chen, S. L., & Abousleiman, Y. N. (2017). Wellbore stability analysis using strain hardening and/or softening plasticity models. *International Journal of Rock Mechanics and Mining Sciences*, 93, 260-268.
- Chen, S. L., Abousleiman, Y. N., & Muraleetharan, K. K. (2012). Closed-form elastoplastic solution for the wellbore problem in strain hardening/softening rock formations. *International Journal of Geomechanics*, 12(4), 494-507.
- Etchecopar, A., P. A. Pezard, and V. Maury. "New borehole imagery techniques: an aid for failure modes and in situ stress analysis and for minimizing drilling incidents." *SPWLA 40th Annual Logging Symposium*. Society of Petrophysicists and Well-Log Analysts, 1999.
- Gaede, O., Karrech, A., & Regenauer-Lieb, K. (2013). Anisotropic damage mechanics as a novel approach to improve pre-and post-failure borehole stability analysis. *Geophysical Journal International*, 193(3), 1095-1109.

9. Ghassemi, A., 2012. A review of some rock mechanics issues in geothermal reservoir development. *Geotech. Geol. Eng.* 30: 647–664.
10. Konstantinovskaya, E., Laskin, P., Ereemeev, D., Pashkov, A., Semkin, A., Karpfinger, F., ... & Trubienko, O. (2016, October). Shale Stability When Drilling Deviated Wells: Geomechanical Modeling of Bedding Plane Weakness, Field X, Russian Platform (Russian). In *SPE Russian Petroleum Technology Conference and Exhibition*. Society of Petroleum Engineers.
11. Labiouse, V., & Vietor, T. (2014). Laboratory and in situ simulation tests of the excavation damaged zone around galleries in Opalinus Clay. *Rock Mechanics and Rock Engineering*, 47(1), 57-70.
12. Lang, J., Li, S., & Zhang, J. (2011, January). Wellbore stability modeling and real-time surveillance for deepwater drilling to weak bedding planes and depleted reservoirs. In *SPE/IADC Drilling Conference and Exhibition*. Society of Petroleum Engineers.
13. Mehrabian, A., Pérez, A. D., & Santana, C. (2018). Wellbore-stability analysis considering the weak bedding planes effect: a case study. *SPE Drilling & Completion*, 33(04), 377-384.
14. Moeck, I., and T. Backers, 2011. Fault reactivation potential as a critical factor during reservoir stimulation. *First Break* 29: 73–80.
15. Okland, D., & Cook, J. M. (1998, January). Bedding-related borehole instability in high-angle wells. In *SPE/ISRM rock mechanics in petroleum engineering*. Society of Petroleum Engineers.
16. Ong, S. H., & Roegiers, J. C. (1993, December). Influence of anisotropies in borehole stability. In *International Journal of Rock Mechanics and Mining Sciences & Geomechanics Abstracts* (Vol. 30, No. 7, pp. 1069-1075). Pergamon.
17. Rutqvist, J. (2012). The geomechanics of CO₂ storage in deep sedimentary formations. *Geotechnical and Geological Engineering*, 30(3), 525-551.
18. Schultz, R. A., Mutlu, U., & Bere, A. (2016, June). Critical issues in subsurface integrity. In *Paper ARMA 16-037 presented at the 50th US Rock Mechanics/Geomechanics Symposium* (Vol. 26, p. 29).
19. Streit, J.E., and R.R. Hillis, 2004. Estimating fault stability and sustainable fluid pressures for underground storage of CO₂ in porous rock. *Energy* 29: 1445–1456.
20. Tellez, C. P., Alcantara Contreras, L., Cabrera, J. R., & Balasejus, D. (2012, January). Pre-Drill WBS Evaluation: Plane of Weakness and Well Design-A Case Study in the South of Mexico. In *IADC/SPE Asia Pacific Drilling Technology Conference and Exhibition*. Society of Petroleum Engineers.
21. Tsopela, A., Bere, A., Dutko, M., Kato, J., (2020). Wellbore stability and predicted cuttings volume in deviated wellbores and bedded formations. *ARMA* 2020-1864
22. Willson, S. M., Edwards, S. T., Crook, A. J., Bere, A., Moos, D., Peska, P., & Last, N. C. (2007, January). Assuring stability in extended reach wells-analyses, practices and mitigations. In *SPE/IADC Drilling Conference*. Society of Petroleum Engineers.
23. Willson, S. M., Last, N. C., Zoback, M. D., & Moos, D. (1999, January). Drilling in South America: a wellbore stability approach for complex geologic conditions. In *Latin American and Caribbean petroleum engineering conference*. Society of Petroleum Engineers.
24. Zhang, J. (2013). Borehole stability analysis accounting for anisotropies in drilling to weak bedding planes. *International journal of rock mechanics and mining sciences*, 60, 160-170.
25. Zhou, J., He, S., Tang, M., Huang, Z., Chen, Y., Chi, J., ... & Yuan, P. (2018). Analysis of wellbore stability considering the effects of bedding planes and anisotropic seepage during drilling horizontal wells in the laminated formation. *Journal of Petroleum Science and Engineering*, 170, 507-524.
26. Zoback, M. D. (2010). *Reservoir geomechanics*. Cambridge University Press.
27. Zoback, M.D., and S.M. Gorelick, 2012. Earthquake triggering and large-scale geologic storage of carbon dioxide. *Proc. US Nat. Acad. Sci.* 109: 10,164–10,168.